

THE FREQUENCY OF DEBRIS DISKS AT WHITE DWARFS

SARA D. BARBER¹, ADAM J. PATTERSON¹, MUKREMIN KILIC¹, S. K. LEGGETT², P. DUFOUR³, J. S. BLOOM⁴, AND D. L. STARR⁴

¹ Homer L. Dodge Department of Physics and Astronomy, University of Oklahoma, 440 W. Brooks St., Norman, OK 73019, USA; barber@nhn.ou.edu

² Gemini Observatory, 670 N. A'ohoku Place, Hilo, HI 96720, USA

³ Département de Physique, Université de Montréal, C.P. 6128, Succursale Centre-Ville, Montréal, Québec H3C 3J7, Canada

⁴ Department of Astronomy, University of California, Berkeley, CA 94720, USA

Received 2012 July 4; accepted 2012 September 13; published 2012 October 31

ABSTRACT

We present near- and mid-infrared photometry and spectroscopy from PAIRITEL, IRTF, and *Spitzer* of a metallicity-unbiased sample of 117 cool, hydrogen-atmosphere white dwarfs (WDs) from the Palomar-Green survey and find five with excess radiation in the infrared, translating to a $4.3^{+2.7}_{-1.2}\%$ frequency of debris disks. This is slightly higher than, but consistent with the results of previous surveys. Using an initial–final mass relation, we apply this result to the progenitor stars of our sample and conclude that 1–7 M_{\odot} stars have at least a 4.3% chance of hosting planets; an indirect probe of the intermediate-mass regime eluding conventional exoplanetary detection methods. Alternatively, we interpret this result as a limit on accretion timescales as a fraction of WD cooling ages; WDs accrete debris from several generations of disks for ~ 10 Myr. The average total mass accreted by these stars ranges from that of 200 km asteroids to Ceres-sized objects, indicating that WDs accrete moons and dwarf planets as well as solar system asteroid analogs.

Key words: infrared: planetary systems – infrared: stars – white dwarfs

Online-only material: color figures

1. INTRODUCTION

The study of extrasolar planetary systems has become a very active field that will continue to grow in the coming years and decades. Over the last two decades, several hundred exoplanets have been discovered, proving planet formation to be a robust process in the Galaxy. The vast majority of known exoplanets have been discovered using just two techniques, namely, radial velocity and transits. To date, radial velocity studies have revealed the presence of well over 500 planets and the number of transiting systems has passed the 200 mark (see <http://exoplanet.eu>; Schneider et al. 2011).

A cursory examination of these planet-hosting stellar systems reveals a curious trend. The frequency of Jovian planets increases from 3% for M dwarfs to 14% for 2 M_{\odot} stars (Johnson et al. 2010; Bowler et al. 2010). In addition, the distribution of known exoplanets as a function of host stellar mass has a strong cutoff at 3 M_{\odot} , above which no exoplanets have been found. Could it be that planets do not form around intermediate-mass stars, or is this a selection effect? The planet formation models of Kennedy & Kenyon (2008) suggest the latter. They predict that the fraction of stars with giant planets shows a steady increase with mass up to 3 M_{\odot} . In addition, the mass of the planets and the width of the regions where they form are predicted to increase with stellar mass. Probing intermediate-mass stellar systems for planets could help test these planet formation models. Since most exoplanet detection methods tend to break down in the intermediate-mass range, one can look at these systems in post-main sequence (MS), where the contrast between the planet's photometric signal and that of its host is greatly decreased. This work examines a sample of white dwarfs (WDs) decedent from 1 to 7 M_{\odot} stars and constrains the frequency of planetary systems in the elusive intermediate-mass regime.

If planets survive post-MS evolution, they should be detectable around WDs (Burleigh et al. 2002; Gould & Kilic 2008). Unfortunately, there are still no confirmed planets around single

WDs. The candidate planet around the pulsating WD GD 66 (Mullally et al. 2007) is currently disputed (J. J. Hermes 2012, private communication). Perhaps an easier way to detect remnant planetary systems around WDs is to look for the tidally disrupted remains of exoplanets and moons in the form of circumstellar debris disks (Debes & Sigurdsson 2002; Jura 2003; Kilic et al. 2006). There are now two dozen WDs known to host dust and/or gas disks. Photospheric abundance analyses of these WDs show that the accreted metals originate from tidally disrupted minor bodies similar in composition to that of bulk Earth (Zuckerman et al. 2007; Klein et al. 2010, 2011; Dufour et al. 2010, 2012). Since at least one giant planet is required to perturb minor bodies out of their stable orbits (Debes et al. 2012), photospheric pollution as well as circumstellar debris disks serve as tracers for giant planets at WDs. Therefore, the frequency of debris disks around WDs can be taken as a lower limit on the frequency of planets around WD remnants of intermediate-mass stars.

The search for debris disks around WDs begins as a search for excess emission in the infrared. Over the last two decades, several hundreds of WDs have been surveyed for infrared excess due to substellar companions or circumstellar disks. The first dusty WD, G29–38, was identified by Zuckerman & Becklin (1987), see also Graham et al. (1990). Zuckerman & Becklin (1992) examined 200 WDs for excesses in the *K* band, while Farihi et al. (2005) surveyed 371 WDs of all spectral types and constrained the frequency of substellar companions to less than 0.5%. The discovery of the second dusty WD, GD 362 (Kilic et al. 2005; Becklin et al. 2005) lead to the realization that dusty WDs may be found more readily by looking at metal-rich WDs.

Previous surveys for debris disks around WDs focused on metal-rich WDs since so far all known WDs with disks also show metal absorption lines in their optical and ultraviolet spectra; DAZ and DBZ spectral types. The Poynting–Robertson drag timescale is significantly shorter than the evolutionary timescales for WDs (von Hippel et al. 2007; Rafikov 2011b),

hence we expect every WD with dust/gas disks to accrete metals from these disks and appear metal-rich. Zuckerman et al. (2003, 2010) find that about 30% of DA and DB WDs show trace amounts of metals in their photospheres. However, only $\sim 20\%$ – 30% of DAZs, the ones with the highest accretion rates, host dust (Kilic et al. 2008; Farihi et al. 2009). The source of metals for the other DAZs remains unknown, but it is likely that the majority of DAZs accrete many small asteroids that do not form a large debris disk (Jura 2008).

Mullally et al. (2007) survey 124 WDs with $T_{\text{eff}} = 5000$ – $170,000$ K using mid-infrared *Spitzer* photometry. Their search for infrared excess finds two dusty WDs for a disk frequency of 1.6%. However, this survey extends beyond the temperature range within which solid dust orbiting interior to the tidal radius can persist. Based on *Spitzer* observations of mostly metal-rich WDs, Farihi et al. (2009) estimate a debris disk frequency of 1%–3% for WDs younger than 500 Myr. Debes et al. (2011) recently searched for infrared excesses among an unbiased (in terms of metallicity) WD sample using the *Wide-field Infrared Survey Explorer* (*WISE*; Wright et al. 2010) data. They found about 1%–5% of these WDs to be dusty. However, the large beam size of *WISE* allows for many false positives due to background contamination, and many of these dusty WD candidates need follow-up higher spatial resolution infrared imaging data to confirm the observed infrared excess.

Here, we present a near- and mid-infrared photometric and spectroscopic survey of an unbiased (in terms of metallicity) sample of DA WDs from the Palomar-Green (PG) survey. Our survey does not focus on metal-rich WDs and thus constrains the disk frequency representative of the general WD population. We target 117 PG WDs with accurate temperature, mass, and age estimates (Liebert et al. 2005) and $T_{\text{eff}} = 9500$ – $22,500$ K. With 117 objects, we sample temperatures at which solid dust can persist within the tidal radius and thus improve upon the constraint obtained by Mullally et al. (2007), whose sample includes 69 WDs in this temperature range. The WDs in our sample are the descendants of MS stars with masses between 1 and $7 M_{\odot}$, so this study extends the search for planets well beyond the mass range available to conventional exoplanet detection methods. Section 2 describes our near- and mid-infrared photometry and spectroscopy data, while Section 3 presents the spectral energy distributions (SEDs) and the dusty WDs in the PG survey. Section 4 presents a discussion of the frequency of disks and planets around WDs and their progenitor MS stars.

2. OBSERVATIONS

2.1. The Sample

Almost all known dusty WDs are relatively young with cooling ages of $\lesssim 1$ Gyr and temperatures in the range 9500–22,500 K (with the exception of G166-58; Farihi et al. 2008). This is probably because a second heavy bombardment phase occurs around intermediate-mass stars in their post-MS evolution due to planetary migration around the mass-losing star (Debes et al. 2012; Bonsor & Wyatt 2012). We would expect to see a peak in the frequency of collisions, tidal disruptions, and disks around the younger WD remnants of such stars (Debes & Sigurdsson 2002).

Consider the disk around G29-38 as a typical system. Jura (2003) models the disk emission and obtains a ring of dust extending from $R_{\text{in}} = 0.1 R_{\odot}$ to $R_{\text{out}} = 0.4$ – $0.9 R_{\odot}$ and $T_{\text{eff}} = 300$ – 600 K. Such a disk around a star twice or three

times as hot as G29-38 would be sublimated and invisible in the IR. That's why our target selection using effective temperature gives a better measurement of the real frequency of disks.

We select 117 apparently single DA WDs from the PG survey with $T_{\text{eff}} = 9500$ – $22,500$ K, where we are most efficient in finding the disks using near- and mid-infrared data. Liebert et al. (2005) performed a detailed model atmosphere analysis of all DA WDs in the PG survey and provided temperature, surface gravity, mass, and age estimates. Their spectroscopy did not have enough resolution to detect the metal-rich DAZs among these targets; our survey does not have a metallicity bias, and hence it has the potential to reveal the true frequency of dusty disks without knowing the fraction of metal-rich WDs among the nearby WD population.

2.2. Near-infrared Photometry

We obtained simultaneous *JHK_s* imaging of 78 WDs using the Peters Automated Infrared Imaging Telescope (PAIRITEL; Bloom et al. 2006) between 2009 February and 2010 April. PAIRITEL is the old Two Micron All Sky Survey (2MASS; Cutri et al. 2003) telescope and it uses the same camera and filter set. The total exposure time for our targets ranged from 70 s to 1500 s depending on the expected brightness of each target. We use the PAIRITEL pipeline version 3.3 processed images and standard IRAF DAOPHOT routines to perform aperture photometry on every 2MASS source detected in the images. We use the 2MASS stars to calibrate the photometry for each object.

Table 1 presents the PAIRITEL photometry (and the 2MASS photometry of a few relatively bright targets) for our sample along with the physical parameters obtained from the model atmosphere analysis of Liebert et al. (2005). We compare our PAIRITEL photometry to that of 2MASS in Figure 1. Only about half of our targets are detected by 2MASS in the *K* band and usually with large photometric errors. Our survey goes significantly deeper than 2MASS and provides improved photometry with smaller errors, which is essential for identifying objects with slight *K*-band excesses. This figure demonstrates that the PAIRITEL photometry agrees fairly well with the 2MASS photometry and that it can be used reliably to constrain the near-infrared SEDs of our targets.

Figure 2 shows *J*–*H* and *J*–*K* colors of our sample of stars as a function of their effective temperatures. The colors for the majority of our targets follow the model predictions of $J - H = J - K \approx 0$ mag, though with some scatter. There are four WDs with *J*–*H* excesses, though with relatively noisy 2MASS photometry. However, from the available mid-infrared photometry from *Spitzer* and/or *WISE*, we conclude that there is no evidence of excess in these objects. The *J*–*H* photometry for the rest of the targets are consistent with the emission from single WDs. Several of these apparently single WDs have positive *J*–*K* colors, suggesting extra emission from a cool companion or a circumstellar debris disk. We chose to further examine those objects with positive *J*–*K* colors by obtaining near-infrared spectra and mid-infrared photometry. Objects with apparently red colors were targeted however, depending on the timing of the observing runs and conditions, some of the objects with blue colors were also followed up as a sanity check.

2.3. Near-infrared Spectroscopy

We obtained low-resolution near-infrared spectra of 41 WDs over several nights in 2011 April, August, and September using the 3 m NASA InfraRed Telescope Facility (IRTF) equipped

Table 1
Sample Properties

PG	T_{eff} (K)	$\log g$	WD Mass (M_{\odot})	MS Mass (M_{\odot})	τ (Myr)	J (mag)	H (mag)	K (mag)	Ref.	Data
0000+172	20210	7.99	0.62	2.1	85	16.262 ± 0.016	16.299 ± 0.035	16.237 ± 0.154	1	I,P
0033+016	10980	8.83	1.12	6.7	2089	15.625 ± 0.014	15.659 ± 0.030	15.649 ± 0.086	1	I,P
0048+202	20160	7.99	0.62	2.1	85	15.795 ± 0.020	15.831 ± 0.041	15.637 ± 0.092	1	I,P
0059+258	21370	8.04	0.65	2.3	78	16.252 ± 0.018	16.266 ± 0.033	16.325 ± 0.135	1	I,P
0107+268	13880	7.87	0.54	1.3	245	15.392 ± 0.015	15.420 ± 0.030	15.528 ± 0.111	1	I,P
0132+254	19960	7.45	0.41	0.1	63	16.446 ± 0.128	1,9	
0816+297	16660	7.84	0.53	1.2	129	16.141 ± 0.105	15.921 ± 0.184	...	1,10	
0819+364	18740	8.03	0.64	2.3	123	16.026 ± 0.088	...	15.781 ± 0.228	1,10	
0821+633	16770	7.82	0.52	1.2	123	16.221 ± 0.009	16.238 ± 0.018	16.342 ± 0.045	1	P
0826+455	10370	7.86	0.52	1.2	513	15.001 ± 0.006	14.947 ± 0.009	14.927 ± 0.018	1	I,S,P
0852+659	19070	8.13	0.70	2.8	141	15.876 ± 0.079	15.826 ± 0.184	...	1,8	
0854+405	22250	7.91	0.58	1.7	46	15.419 ± 0.009	15.496 ± 0.014	15.553 ± 0.029	1	I,P
0908+171	17340	7.92	0.57	1.6	129	16.403 ± 0.013	16.458 ± 0.024	16.573 ± 0.064	1	P
0915+526	15560	7.96	0.60	1.9	200	15.809 ± 0.009	15.894 ± 0.018	15.977 ± 0.039	1	P
0933+729	17380	8.00	0.62	2.1	148	16.074 ± 0.009	16.067 ± 0.018	16.108 ± 0.045	1	P
0938+286	14490	7.82	0.52	1.2	200	15.742 ± 0.016	15.750 ± 0.027	15.924 ± 0.060	1	P
0938+550	18530	8.10	0.68	2.6	148	15.153 ± 0.025	15.306 ± 0.033	15.396 ± 0.053	1	I,P
0943+441	12820	7.55	0.41	0.1	339	13.643 ± 0.028	13.707 ± 0.041	13.722 ± 0.046	1,9	
0947+326	22060	8.31	0.82	3.9	117	16.022 ± 0.015	16.044 ± 0.023	15.841 ± 0.069	1	I,P
0950+078	14770	7.95	0.59	1.8	229	16.148 ± 0.011	16.280 ± 0.021	16.280 ± 0.049	1	P
0954+697	21420	7.91	0.58	1.7	54	16.427 ± 0.016	16.612 ± 0.042	16.548 ± 0.078	1	P
0956+021	15670	7.80	0.51	1.1	151	16.007 ± 0.012	16.073 ± 0.022	16.130 ± 0.049	1	S,P
1000-002	19470	7.99	0.62	2.1	98	16.474 ± 0.019	16.558 ± 0.054	16.614 ± 0.094	1	P
1003-023	20340	7.95	0.60	1.9	76	15.677 ± 0.014	15.733 ± 0.030	15.845 ± 0.057	1	P
1005+642	19660	7.93	0.58	1.7	81	14.232 ± 0.029	14.330 ± 0.050	14.356 ± 0.052	1	
1015+161	19540	8.04	0.65	2.3	110	15.950 ± 0.010	15.944 ± 0.018	15.906 ± 0.036	1,4	P
1017+125	21670	7.94	0.60	1.9	56	16.236 ± 0.096	15.856 ± 0.177	15.875 ± 0.253	1,10	
1019+129	18020	8.00	0.62	2.1	132	16.101 ± 0.017	16.048 ± 0.031	15.981 ± 0.058	1	I,P
1022+050	11680	7.64	0.44	0.4	490	14.193 ± 0.035	14.237 ± 0.033	14.185 ± 0.065	1	
1026+024	12570	7.98	0.60	1.9	363	14.433 ± 0.011	14.447 ± 0.017	14.362 ± 0.031	1	I,P
1031+063	20750	7.87	0.56	1.5	58	16.726 ± 0.025	16.912 ± 0.061	16.647 ± 0.093	1	I,P
1031+234	15000	8.50	0.93	4.9	550	16.044 ± 0.009	16.108 ± 0.016	16.123 ± 0.049	1	P
1034+492	20650	8.17	0.73	3.1	11	15.778 ± 0.063	16.127 ± 0.212	16.061 ± 0.287	1,8	
1036+086	22230	7.49	0.42	0.2	46	16.654 ± 0.015	16.810 ± 0.034	16.471 ± 0.066	1	I,S,P
1046+282	12610	7.97	0.59	1.8	363	15.479 ± 0.016	15.438 ± 0.028	15.349 ± 0.057	1	I,P
1102+749	19710	8.36	0.85	4.2	182	15.530 ± 0.010	15.574 ± 0.023	15.746 ± 0.044	1	P
1108+476	12400	8.31	0.80	3.7	603	15.657 ± 0.054	15.350 ± 0.092	15.618 ± 0.222	1,8	
1115+166	22090	8.12	0.70	2.8	81	15.466 ± 0.055	15.657 ± 0.159	15.463 ± 0.208	1	
1116+026	12290	8.05	0.63	2.2	427	14.745 ± 0.014	14.668 ± 0.021	14.718 ± 0.032	1,4	P
1122+546	14380	7.83	0.52	1.2	209	15.697 ± 0.015	15.704 ± 0.034	15.590 ± 0.053	1	I,S,P
1129+072	13360	7.91	0.56	1.5	288	15.298 ± 0.012	15.158 ± 0.018	15.266 ± 0.033	1	P
1129+156	16890	8.19	0.73	3.1	224	14.443 ± 0.034	14.493 ± 0.052	14.565 ± 0.094	1,8	
1134+301	21280	8.55	0.96	5.2	200	12.993 ± 0.024	13.105 ± 0.031	13.183 ± 0.028	3	
1147+256	10200	8.14	0.69	2.7	794	15.548 ± 0.012	15.555 ± 0.020	15.668 ± 0.047	1	P
1149+058	11070	8.15	0.69	2.7	646	14.985 ± 0.015	14.962 ± 0.021	14.861 ± 0.035	1	I,S,P
1149+411	14070	7.84	0.53	1.2	224	16.365 ± 0.017	16.431 ± 0.037	16.398 ± 0.064	1	P
1158+433	14050	7.85	0.53	1.2	224	16.170 ± 0.011	16.197 ± 0.020	16.169 ± 0.043	1	P
1159-098	9540	8.81	1.10	6.5	2692	15.533 ± 0.018	15.491 ± 0.032	15.419 ± 0.090	1	I,P
1201-001	19770	8.26	0.78	3.5	155	15.680 ± 0.057	15.846 ± 0.098	15.706 ± 0.231	1,8	
1216+036	13800	7.85	0.53	1.2	245	16.284 ± 0.101	16.198 ± 0.187	...	1,10	
1229-013	19430	7.47	0.41	0.1	71	14.925 ± 0.032	15.044 ± 0.070	15.349 ± 0.229	1,9	
1230+418	19520	7.98	0.61	2.0	95	16.161 ± 0.014	16.180 ± 0.027	16.337 ± 0.055	1	P
1232+479	14370	7.82	0.52	1.2	204	14.937 ± 0.011	14.760 ± 0.014	14.725 ± 0.024	1	I,P
1237-029	10240	8.58	0.98	5.4	1660	15.828 ± 0.011	15.761 ± 0.018	15.955 ± 0.040	1	P
1244+149	10680	8.06	0.64	2.3	631	15.740 ± 0.015	15.714 ± 0.029	15.729 ± 0.058	1	P
1257+032	17290	7.79	0.51	1.1	105	16.090 ± 0.092	15.956 ± 0.159	...	1,10	
1258+593	14480	7.87	0.54	1.3	214	15.645 ± 0.012	15.607 ± 0.021	15.621 ± 0.051	1	P
1307+354	11180	8.15	0.70	2.8	631	15.344 ± 0.051	15.398 ± 0.096	...	1,8	
1310+583	10560	8.32	0.80	3.7	912	14.016 ± 0.028	14.004 ± 0.045	14.081 ± 0.073	1,8	
1319+466	13880	8.19	0.73	3.1	398	14.867 ± 0.035	14.859 ± 0.075	14.767 ± 0.083	1,8	
1325+168	17970	8.18	0.73	3.1	186	16.426 ± 0.016	16.640 ± 0.045	16.499 ± 0.063	1	I,S,P
1328+344	16300	7.90	0.56	1.5	155	15.495 ± 0.008	15.528 ± 0.015	15.654 ± 0.030	1	P
1330+473	22460	7.95	0.60	1.9	48	15.772 ± 0.011	15.710 ± 0.017	15.912 ± 0.042	1	P
1335+369	20510	7.78	0.51	1.1	51	15.122 ± 0.010	15.152 ± 0.016	15.188 ± 0.029	1	P
1337+705	20460	7.90	0.57	1.6	66	13.248 ± 0.024	13.357 ± 0.027	13.451 ± 0.035	1,3,	

Table 1
(Continued)

PG	T_{eff} (K)	$\log g$	WD Mass (M_{\odot})	MS Mass (M_{\odot})	τ (Myr)	J (mag)	H (mag)	K (mag)	Ref.	Data
1344+573	13390	7.94	0.58	1.7	295	13.704 ± 0.022	13.821 ± 0.035	13.757 ± 0.041	1	
1349+144	16620	7.68	0.46	0.6	145	15.550 ± 0.009	15.629 ± 0.017	15.664 ± 0.036	1	P
1349+552	11800	7.87	0.54	1.3	380	15.830 ± 0.015	15.967 ± 0.028	15.800 ± 0.060	1	I,P
1350+657	11880	7.91	0.55	1.4	389	15.688 ± 0.068	15.419 ± 0.136	15.304 ± 0.175	1	
1350-090	9520	8.36	0.83	4.0	1318	14.191 ± 0.007	14.082 ± 0.009	14.140 ± 0.013	1	P
1407+425	10010	8.21	0.73	3.1	912	14.998 ± 0.044	14.870 ± 0.064	14.892 ± 0.095	1,5	
1408+324	18150	7.95	0.59	1.8	117	14.396 ± 0.031	14.484 ± 0.054	14.431 ± 0.073	3	
1410+425	15350	7.87	0.54	1.3	178	16.343 ± 0.016	16.337 ± 0.025	16.467 ± 0.069	1	P
1431+154	13550	7.95	0.58	1.7	302	16.130 ± 0.014	15.985 ± 0.022	15.895 ± 0.053	1	I,P
1448+078	14170	7.75	0.48	0.8	195	15.854 ± 0.016	15.755 ± 0.027	15.788 ± 0.072	1	I,P
1449+168	21600	7.88	0.56	1.5	49	15.973 ± 0.010	16.077 ± 0.018	15.861 ± 0.044	1	I,P
1457-086	21450	7.97	0.62	2.1	63	16.041 ± 0.098	16.212 ± 0.233	15.614 ± 0.228	1,7	
1501+032	13770	7.88	0.54	1.3	257	15.856 ± 0.018	15.847 ± 0.033	15.900 ± 0.063	1	P
1502+351	18120	8.13	0.70	2.8	166	16.239 ± 0.024	16.386 ± 0.038	16.305 ± 0.072	1	I,P
1507+021	19580	7.87	0.56	1.5	76	16.601 ± 0.115	16.451 ± 0.209	...	1,10	
1507+220	19340	7.91	0.57	1.6	85	15.445 ± 0.015	15.525 ± 0.021	15.698 ± 0.055	1	P
1508+549	16970	7.86	0.54	1.3	126	16.125 ± 0.009	16.136 ± 0.019	16.278 ± 0.051	1	P
1508+637	10450	8.12	0.68	2.6	724	14.689 ± 0.015	14.660 ± 0.023	14.823 ± 0.046	1	P
1509+323	13970	7.98	0.60	1.9	282	14.436 ± 0.030	14.574 ± 0.055	14.572 ± 0.089	3	
1515+669	10320	8.40	0.86	4.3	1122	15.295 ± 0.053	15.240 ± 0.112	15.180 ± 0.198	1,8	
1519+384	19620	7.98	0.61	2.0	93	16.207 ± 0.015	16.359 ± 0.032	16.176 ± 0.080	1	I,P
1527+091	21520	8.02	0.64	2.3	71	14.814 ± 0.012	14.922 ± 0.018	15.003 ± 0.037	1	P
1531-023	18620	8.41	0.88	4.5	234	14.395 ± 0.040	14.484 ± 0.053	14.618 ± 0.101	3	
1533-057	20000	8.50	0.94	5.0	245	15.876 ± 0.013	15.951 ± 0.031	16.082 ± 0.059	1	P
1537+652	9740	8.15	0.69	2.7	912	14.438 ± 0.006	14.426 ± 0.009	14.372 ± 0.014	1	IP
1541+651	11600	8.10	0.67	2.5	537	15.625 ± 0.013	15.590 ± 0.025	15.450 ± 0.048	1	I,S,P
1548+149	20520	7.89	0.57	1.6	65	15.656 ± 0.013	15.844 ± 0.029	15.821 ± 0.061	1	IP
1550+183	14260	8.25	0.77	3.4	389	15.170 ± 0.050	15.311 ± 0.107	15.278 ± 0.131	1,8	
1601+581	14670	7.84	0.53	1.2	200	14.116 ± 0.010	14.151 ± 0.013	14.209 ± 0.021	1	P
1605+684	21090	7.97	0.61	2.0	68	16.404 ± 0.010	16.474 ± 0.026	16.276 ± 0.054	1	S,P
1610+167	14390	7.84	0.52	1.2	209	16.047 ± 0.011	16.033 ± 0.024	16.027 ± 0.065	1	I,P
1614+137	22430	7.33	0.40	0.1	30	15.704 ± 0.059	15.896 ± 0.141	...	1	
1620+513	20890	7.92	0.58	1.7	63	16.251 ± 0.093	16.181 ± 0.213	...	1,10	
1626+409	21370	8.02	0.64	2.3	72	16.647 ± 0.027	16.933 ± 0.068	16.851 ± 0.146	1	I,P
1632+177	10100	7.96	0.58	1.7	617	13.049 ± 0.021	12.989 ± 0.027	13.076 ± 0.029	1,5	
1637+335	10150	8.17	0.71	2.9	832	14.551 ± 0.031	14.467 ± 0.045	14.424 ± 0.081	3	
1641+388	15570	7.95	0.59	1.8	195	14.958 ± 0.008	15.066 ± 0.014	15.024 ± 0.037	1	I,P
1647+376	21980	7.89	0.57	1.6	46	15.494 ± 0.007	15.533 ± 0.016	15.782 ± 0.051	1	I,P
1654+637	15070	7.63	0.44	0.4	204	16.167 ± 0.103	15.688 ± 0.146	15.565 ± 0.179	1,9	
1659+303	13600	7.95	0.58	1.7	295	15.315 ± 0.011	15.328 ± 0.025	15.435 ± 0.045	1	IP
1720+361	13670	7.83	0.52	1.2	245	15.476 ± 0.023	15.592 ± 0.046	15.136 ± 0.075	1	I,S,P
2226+061	15280	7.62	0.44	0.4	191	15.178 ± 0.045	15.217 ± 0.067	15.227 ± 0.142	1,9	
2246+223	10650	8.80	1.10	6.5	2188	14.341 ± 0.029	14.317 ± 0.047	14.360 ± 0.090	3	
2303+243	11480	8.09	0.66	2.4	550	15.398 ± 0.028	15.509 ± 0.042	15.363 ± 0.073	1	S,P
2306+125	20220	8.05	0.66	2.4	98	15.672 ± 0.012	15.642 ± 0.024	15.735 ± 0.068	1	I,P
2306+131	13250	7.92	0.56	1.5	295	15.567 ± 0.013	15.553 ± 0.026	15.299 ± 0.065	1	I,S,P
2322+207	13060	7.84	0.52	1.2	282	15.745 ± 0.013	15.708 ± 0.026	15.354 ± 0.066	1	I,P
2324+060	15750	7.90	0.56	1.5	174	15.744 ± 0.028	15.879 ± 0.063	16.051 ± 0.249	1	I,P
2326+049	11820	8.15	0.70	2.8	550	13.132 ± 0.029	13.075 ± 0.022	12.689 ± 0.029	1,2,3,5,6	
2328+108	21910	7.84	0.55	1.4	42	15.900 ± 0.013	15.911 ± 0.023	16.046 ± 0.109	1	I,P
2329+267	11730	8.98	1.18	7.2	2042	15.126 ± 0.011	15.093 ± 0.020	14.908 ± 0.088	1	I,P
2336+063	16520	8.03	0.63	2.2	186	15.903 ± 0.017	15.959 ± 0.032	16.140 ± 0.135	1	I,P

Note. Data sources: (I) IRTF; (S) *Spitzer*; (P) PAIRITEL.

References. (1) This work; (2) Reach et al. 2005; (3) Mullally et al. 2007; (4) Jura et al. 2007; (5) Farihi et al. 2008; (6) Reach et al. 2009; (7) Farihi et al. 2009; (8) Kilic et al. 2009a; (9) Kilic et al. 2010; (10) Xu & Jura 2012.

with the 0.8–5.4 Micron Medium-Resolution Spectrograph and Imager (SpeX; Rayner et al. 2003). The observing setup and procedures are similar to those of Kilic et al. (2012). We use a 0.5 slit to obtain a resolving power of 90–210 over the 0.7–2.5 μm range. The observations are taken in two different positions on the slit separated by 10". We use internal calibration

lamps (a 0.1 W incandescent lamp and an argon lamp) for flat fielding and wavelength calibration, respectively. To correct for telluric features and flux calibrate the spectra, we use the observations of nearby A0V stars at a similar airmass to the target observations. We use the IDL-based package SPEXTOOL version 3.4 (Cushing et al. 2004) to reduce the data.

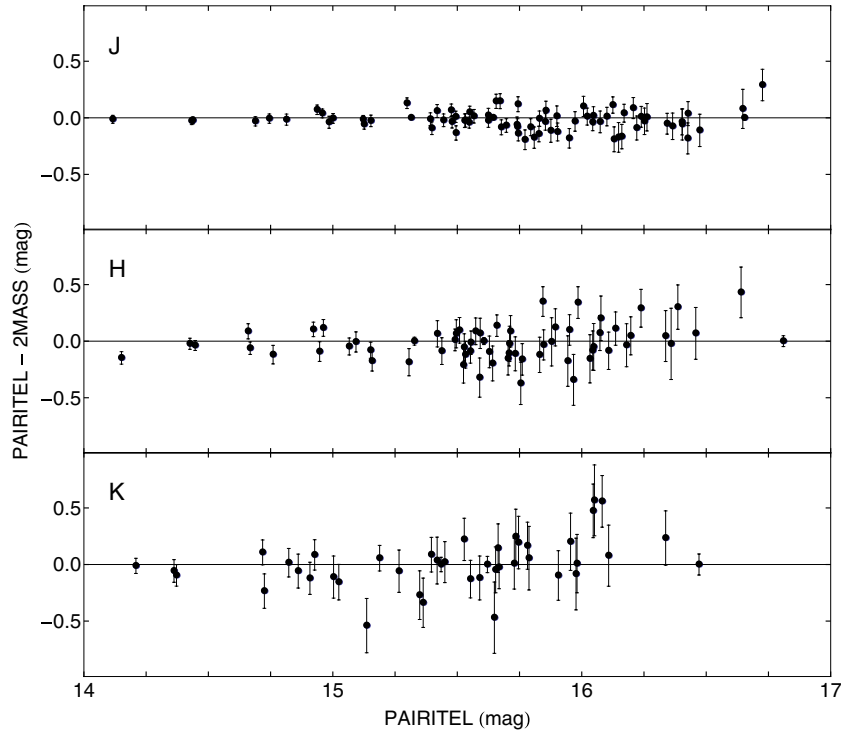


Figure 1. PAIRITEL vs. 2MASS photometry for our sample. The PAIRITEL data agree fairly well with the 2MASS photometry.

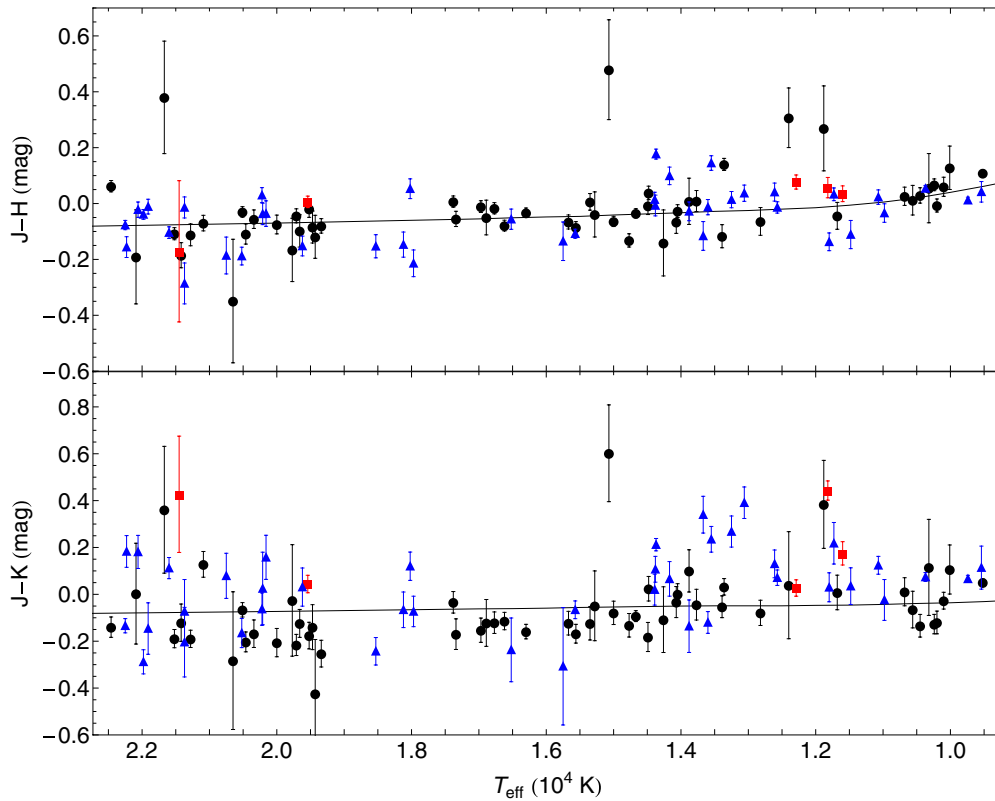


Figure 2. $J-H$ and $J-K$ colors vs. temperature for our sample of DA WDs from the PG survey. Red squares and blue triangles show the confirmed dusty WDs and objects with follow-up IRTF spectroscopy, respectively. Solid lines show the predicted sequences for DA WDs (Bergeron et al. 2011).

(A color version of this figure is available in the online journal.)

To demonstrate that our near-infrared observations and reductions are reliable, we also obtained a near-infrared spectrum of the previously known dusty WD GALEX J193156.8+011745 (hereafter J1931+0117; Vennes et al. 2010; Debes et al. 2011;

Melis et al. 2011). Figure 3 shows the near-infrared photometry and our IRTF spectrum of this object. There are two nearby red sources within $2''$ of the WD (Melis et al. 2011). Our IRTF observations were obtained under average seeing conditions of $0''.8$

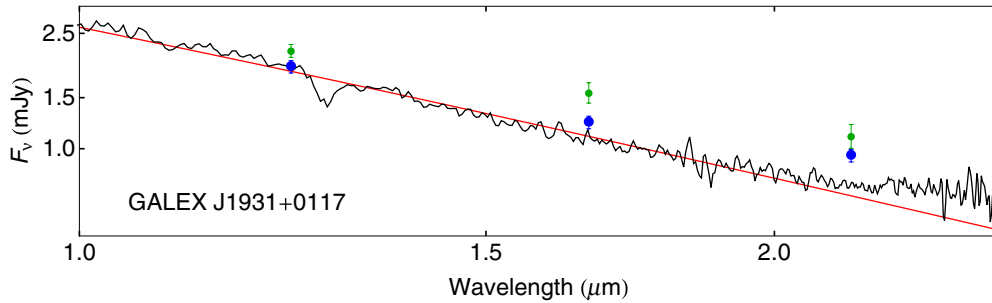


Figure 3. Spectral energy distribution of the known dusty WD GALEX J1931+0117. Green points represent 2MASS photometry, while blue points represent the photometry from Melis et al. (2011). The IRTF spectrum is shown in black and the red line represents the predicted contribution from a blackbody stellar photosphere. The noise near 1.9 and 2.5 μm falls in regions of poor telluric correction. The 1.28 μm feature is Pa β absorption. The detection of slight K -band excess around this target demonstrates that our near-infrared observations and reductions are reliable.

(A color version of this figure is available in the online journal.)

and our 0.5 slit minimizes the contamination from the nearby sources. A slight excess is clearly detected redward of 2.1 μm , typical of dusty WDs (Kilic et al. 2006). Melis et al. (2011) also obtained a near-infrared spectrum of J1931+0117 on the Magellan 6.5 m Baade telescope, which shows a significantly larger excess redward of 1.6 μm . Those authors discuss the potential problems with the flux calibration of their spectra. They model the excess around J1931+0117 with a flat disk model with inner and outer temperatures of 1400 and 1200 K, essentially a narrow ring of dust. Our IRTF spectrum demonstrates that the excess around J1931+0117 mostly shows up redward of 2.1 μm and it is similar to the other dusty WDs with extended (up to 1 R_{\odot}) disks. Of course, the outer edge of the disk around J1931+0117 is currently unconstrained due to the lack of uncontaminated mid-infrared photometry. Regardless of these issues, this figure demonstrates that we are able to identify dusty WDs even with slight K -band excesses.

2.4. *Spitzer* Photometry

We used the warm *Spitzer* equipped with the InfraRed Array Camera (IRAC; Fazio et al. 2004) to obtain infrared photometry of 11 WDs between 2010 September and 2011 February for program number 70023. Based on our preliminary analysis of the PAIRITEL data, these 11 sources appeared to have slight K -band excesses indicative of debris disks. We obtained 3.6 and 4.5 μm images with integration times of 30 s or 100 s for nine dither positions. We use the IDL ASTROLIB packages to perform aperture photometry on the individual corrected basic calibrated data frames from the S18.18.0 pipeline reduction.

Following the IRAC calibration procedures, we correct for the location of the source in the array before averaging the fluxes of each of the dithered frames at each wavelength. We also correct the Channel 1 (3.6 μm) photometry for the pixel phase dependence. We estimate the photometry error bars from the observed scatter in the nine images corresponding to the dither positions. We add the 3% absolute calibration error in quadrature (Reach et al. 2005). Finally, we divide the estimated fluxes by the color corrections for a Rayleigh–Jeans spectrum, except for the dusty WDs in our sample. Table 2 presents our *Spitzer* IRAC photometry for 11 PG WDs.

3. RESULTS

Our near-infrared photometric observations revealed several sources with potential K -band excesses. We followed up 11 of the most interesting targets with *Spitzer* IRAC and 41 stars in total at the IRTF. Figure 4 shows the SEDs of the 41 stars

Table 2
Spitzer IRAC Photometry

PG	3.6 μm (μJy)	4.5 μm (μJy)
0826+455	268.6 \pm 8.7	172.0 \pm 5.9
0956+021	88.6 \pm 3.5	53.7 \pm 2.8
1036+086	42.5 \pm 1.5	26.6 \pm 1.3
1122+546	118.2 \pm 4.3	77.6 \pm 3.1
1149+058	248.0 \pm 8.1	163.4 \pm 5.7
1325+168	64.7 \pm 2.2	42.3 \pm 1.7
1541+651	435.4 \pm 13.5	483.9 \pm 15
1605+684	60.9 \pm 2.7	41.2 \pm 2.2
1720+361	155.9 \pm 5.4	97.6 \pm 3.7
2303+243	170.8 \pm 5.9	110.1 \pm 4
2306+131	146.2 \pm 5.2	92.0 \pm 3.5

Note. *Spitzer* Cycle 7 photometry fluxes in IRAC Channels 1 (3.6 μm) and 2 (4.5 μm).

observed at the IRTF. Here, and in the rest of the figures, the PAIRITEL and 2MASS photometry are shown as blue and green points, respectively. The black lines show the observed spectra and the red solid lines show the predicted photospheric emission for each star assuming a blackbody. The IRTF spectra display telluric correction problems around 1.4 and 1.9 μm , but otherwise they closely follow the predicted blackbody distributions for the majority of the targets in our sample. PG 0048+202 and PG 1720+361 are two of the stars for which our PAIRITEL photometry indicated K -band excesses, but our IRTF spectra show that there are no significant excesses in the K band for these two stars. There is only one WD in our IRTF sample, where a significant K -band excess is detected, PG 1541+651. The observed flux stays essentially constant between 2.0 and 2.5 μm , which is typical of dusty WDs. The detection of Ca II 3933 \AA absorption in the HIRES spectrum of this object (S. Xu et al. 2012, in preparation) corroborates the presence of circumstellar debris.

Figure 5 shows the near- and mid-infrared data on 11 WDs that we targeted with *Spitzer*, including PG 1541+651. Eight of these stars also have IRTF spectroscopy available. Our *Spitzer* observations confirm the results from the IRTF observations; only PG 1541+651 shows a significant infrared excess that is compatible with a debris disk (see Kilic et al. 2012). The SEDs for the other 10 objects in this figure are consistent with photospheric emission from each star.

There are four other previously known dusty WDs in our sample; PG 1015+161, PG 1116+026, PG 1457–086, and

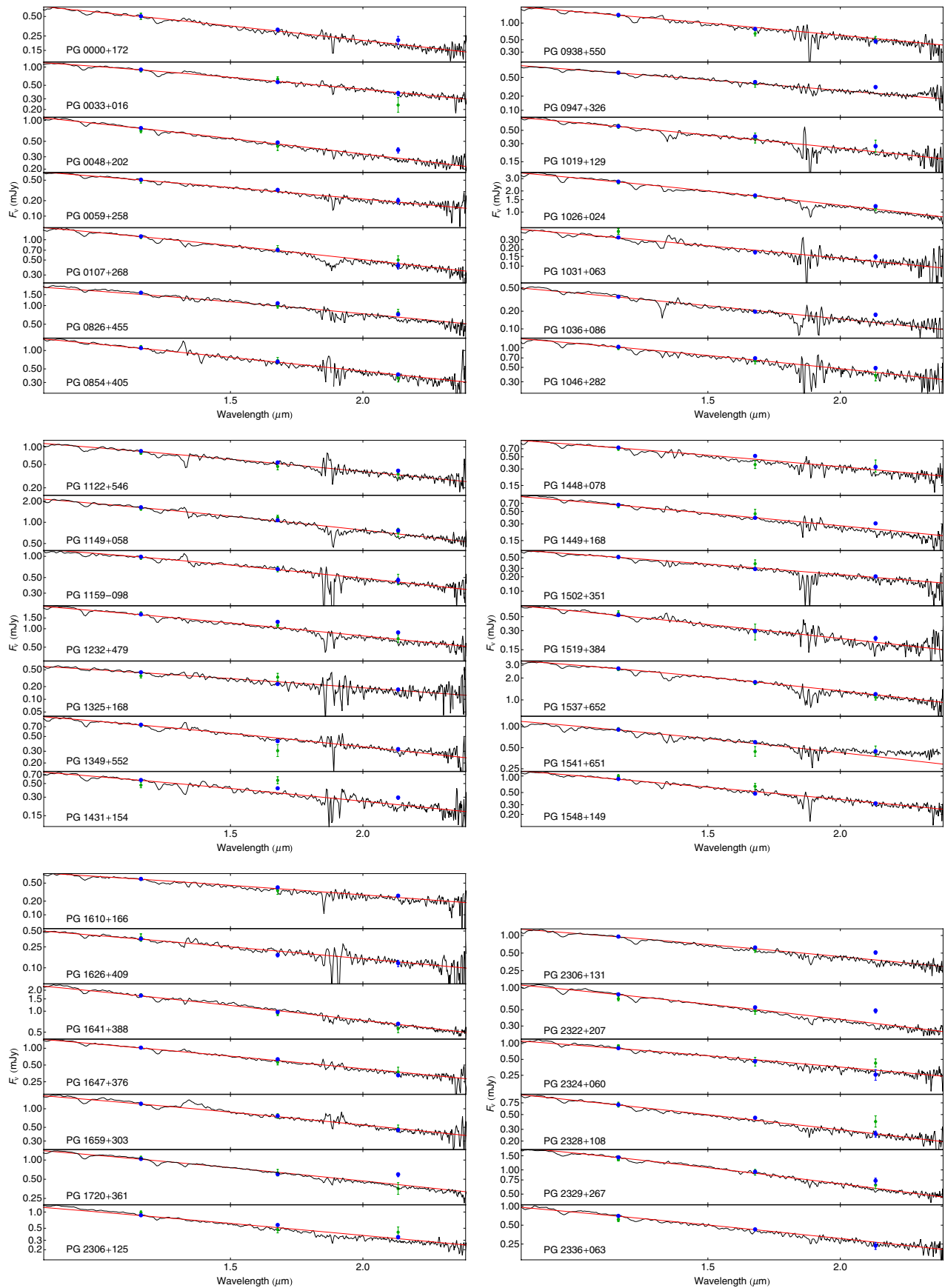


Figure 4. Spectral energy distributions of 41 WDs observed at the IRTF. The PAIRITEL and 2MASS photometry are shown as blue and green points, respectively. The black lines show the observed spectra and the red solid lines show the predicted photospheric emission for each star assuming a blackbody. The IRTF spectra display telluric correction problems around 1.4 and 1.9 μm .

(A color version of this figure is available in the online journal.)

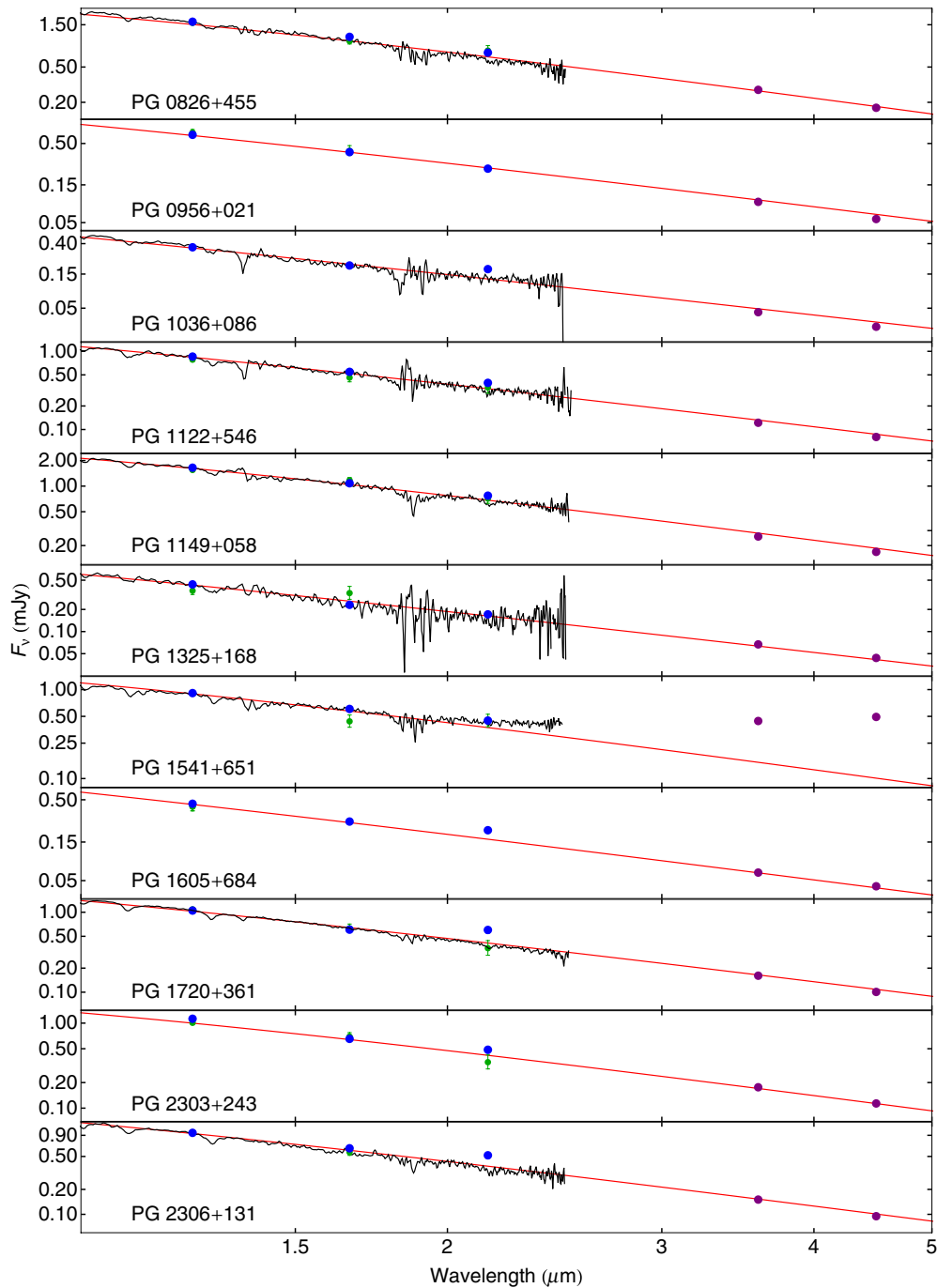


Figure 5. SEDs of the 11 WDs with new *Spitzer* photometry (shown in purple). The symbols are the same as in Figure 3. The IRTF spectra display telluric correction problems around 1.4 and 1.9 μm . Our *Spitzer* observations confirm the results of the IRTF observations; only PG1541+651 shows a significant infrared excess. (A color version of this figure is available in the online journal.)

PG 2326+049. Figure 6 displays the SEDs for these four WDs plus PG 1541+651. PG 2326+049 has the most prominent excess, while the excess at PG 1457–086 is the most subtle. The variation in the strength of these excesses is likely due to a variation in the disk geometry from object to object. There is another known dusty WD in the Liebert et al. (2005) DA WD sample, PG 1456+298 (G166-58; Farihi et al. 2008), that is cooler than the lower temperature limit of our sample and hence it is not included in Figure 6.

Out of the 117 DA WDs in our sample, the majority have SEDs that closely follow a single blackbody curve, while five

WDs show a significant deviation from their blackbody model in the near- to mid-infrared (see Figure 6). In light of the recent *WISE* All-Sky Data Release, we examine our sample of objects for infrared excesses in the *WISE* data and plot these results in Figure 7. Four of the five dusty WDs in our sample clearly show infrared excesses in the *WISE* bands. The fifth dusty WD, PG 1457–086, is also detected in the *WISE* observations, but with large photometric errors. There is another target, PG 1519+384, with positive $H - W1$ and $H - W2$ colors. However, there are two nearby sources within several arcseconds of this target in the Sloan Digital Sky Survey images. The *WISE*

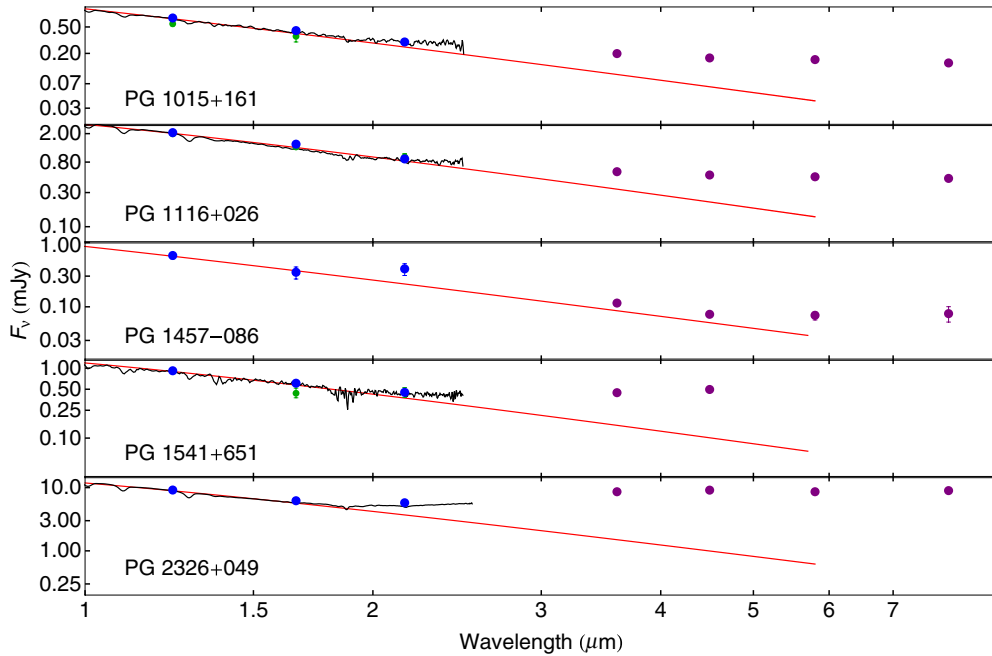


Figure 6. SEDs of the five dusty WDs in our sample. The symbols are the same as in Figure 5. The IRTF spectra display telluric correction problems around 1.4 and 1.9 μm .

(A color version of this figure is available in the online journal.)

photometry for PG 1519+384 is likely contaminated by these background sources. Hence, the *WISE* data do not reveal any new dusty WDs in our sample other than the five systems known.

Farihi et al. (2005) finds a frequency of less than 0.5% for brown dwarf companions of WDs. Given our sample size of 117, we would expect to find less than one brown dwarf companion in our sample. It is not surprising, then, that we do not find any substellar companions. Through the initial selection process, we excluded objects with potential M dwarf companions.

4. DISCUSSION

4.1. The Frequency of Debris Disks Around WDs

Out of the 348 DA WDs analyzed by Liebert et al. (2005), 308 are apparently single. Six of these PG WDs are known to host dust disks, corresponding to a debris disk frequency of 1.9%. This is similar to the frequency of disks, 1.6%, around the nearby bright WD sample of Mullally et al. (2007). Of course, these estimates ignore the fact that most disks occur around young WDs (see Kilic et al. 2009b). The process that creates the debris disks around WDs seems to be more efficient at younger ages.

We use the binomial probability distribution to compute the upper and lower limits on the frequency (p) of disks. The binomial distribution function gives the discrete probability distribution of obtaining exactly n successes out of N trials (where the result of each trial is true with probability p and false with probability $1 - p$). The probability, $P_n(N, p)$, that a survey of N WDs will detect n debris disks, when the true frequency of disks is p is given by (Burgasser et al. 2003, Appendix)

$$P_n(N, p) = \binom{N}{n} p^n (1 - p)^{N-n} = \frac{N!}{n!(N-n)!} p^n (1 - p)^{N-n}. \quad (1)$$

Since this probability function is not symmetric about its maximum value, we report the range in p that delimits 68% of

the integrated probability function, equivalent to 1σ Gaussian limits. For $N = 117$ and $n = 5$, there is a 68% chance of p being between 3.1% and 7% (see Figure 8). Thus, $p = 4.3^{+2.7}_{-1.2}\%$. This frequency estimate is slightly higher than, but consistent with, the 3% disk frequency derived by Farihi et al. (2009).

Girven et al. (2011) and Steele et al. (2011) use UKIDSS data to arrive at a disk frequency of $\sim 1\%$. Similarly, Farihi et al. (2012) use warm *Spitzer* data to obtain a frequency of dust disks at DA WDs of at least 0.8% for stars with cooling ages of less than 1 Gyr. These estimates are lower than our 4.3% estimate, but they are consistent within the errors. Since our survey focuses on relatively bright targets, it is easier to identify potential sources with near- and mid-infrared excesses.

4.2. Planets Around Intermediate-mass Stars

The 117 WDs in our sample have an average mass of $0.6 M_\odot$ and mass range of $0.4\text{--}1.2 M_\odot$. We estimate the progenitor MS masses using the initial–final mass relation derived by Kalirai et al. (2008) and Williams et al. (2009). We obtain an average progenitor mass of $2.4 M_\odot$ and mass range of $1.1\text{--}7.2 M_\odot$ (see Table 1), where we neglect WDs below $0.5 M_\odot$. Based on the observed frequency of disks around our WD targets, we find that the probability of finding planetary systems around their progenitor $1\text{--}7 M_\odot$ MS stars is at least $4.3^{+2.7}_{-1.2}\%$. This result serves as an indirect probe of the intermediate-mass stellar systems, which have thus far challenged conventional planetary detection techniques (Gould & Kilic 2008).

The dusty WDs in our sample, PG 1015+161, 1116+026, 1457–086, 1541+651, and 2326+049, are the descendants of $2.1\text{--}2.8 M_\odot$ MS stars. At first glance, this argues that planet formation may be most efficient around $2\text{--}3 M_\odot$ stars. However, given the age and star formation history of the Galactic disk, our sample is dominated by the $\sim 0.6 M_\odot$ WD remnants of $2\text{--}3 M_\odot$ MS stars. In fact, 80% of our sample consists of WD descendants of $1\text{--}3 M_\odot$ MS stars. Hence, the lack of discoveries of dusty disks, and therefore remnant planetary systems, around

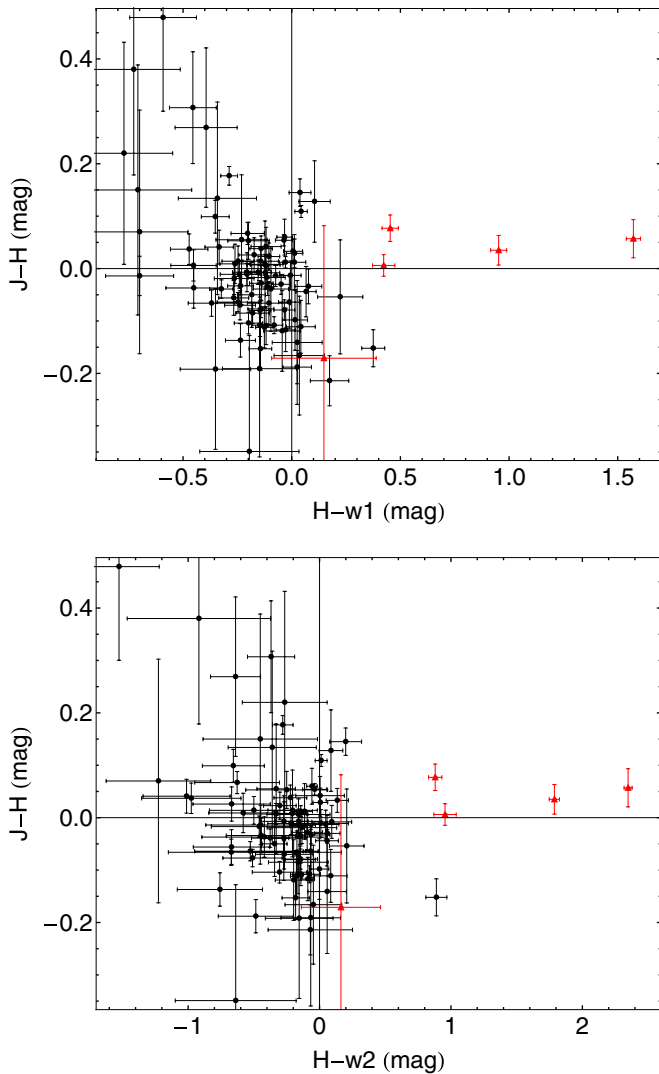


Figure 7. Color–color diagrams using PAIRITEL/2MASS and *WISE* photometry for our WD sample. Red triangles mark the dusty WDs. Four of the five dusty WDs in our sample clearly show infrared excesses in the *WISE* bands. The fifth dusty WD, PG 1457–086, is also detected in the *WISE* observations, but with large photometric errors.

(A color version of this figure is available in the online journal.)

the massive WD remnants of $M > 3 M_{\odot}$ stars may be due to small number statistics. There are 22 systems in our sample with $M > 3 M_{\odot}$ progenitors, we would expect to find one dusty WD in a sample of 22 stars. The probability of finding zero dusty WDs in a sample of 22, when the expected number is one, is 30% see Equation (1). Hence, larger surveys of massive WDs are required to detect disks around them and to constrain the frequency of planets around their intermediate-mass progenitor MS stars.

4.3. Disk Lifetimes

An alternative interpretation of the 4.3% disk frequency around WDs is that perhaps 100% of WDs have remnant planetary systems that can create debris disks, but the disks only persist for 4.3% of the cooling age of the WD. For the average cooling age of our sample of WDs, 300 Myr, this implies that disks survive around typical WDs for ~ 10 Myr. We note that this is the total time a WD accretes from circumstellar debris disks, even though individual disks may last for a significantly

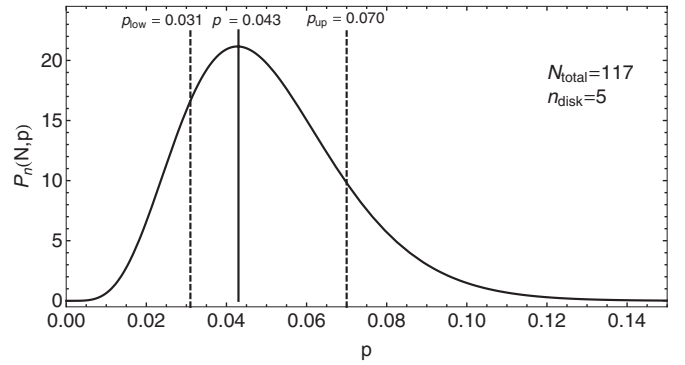


Figure 8. Probability function for WDs with debris disks. Probability, $P_n(N, p)$, of finding $n = 5$ debris disks as a function of assumed true debris disk frequencies, p , where $N = 117$. Dashed lines delineate the region containing 68% probability, equivalent to 1σ Gaussian limits. The solid line indicates the peak of the distribution. The derived frequency is $4.3^{+2.7}_{-1.2}\%$.

shorter amount of time. Kilic et al. (2008) and Farihi et al. (2009) estimate typical disk lifetimes of $\sim 10^5$ years. Hence, up to 100 tidal disruption events that create circumstellar debris disks may occur for any given WD.

von Hippel et al. (2007) use a geometrically thin, optically thick disk model to determine typical accretion rates of WDs. Their result ($\sim 10^9$ g s $^{-1}$) means a WD with the disk lifetime typical of our sample will accrete a total mass equivalent to a 400 km solar system asteroid (assuming an asteroid density of 3 g cm $^{-3}$). Rafikov (2011a) demonstrate that the Poynting–Robertson drag can explain accretion rates of around 10^8 g s $^{-1}$ from circumstellar debris disks onto the WDs. Taken at face value, this implies a total accreted mass of 10^{22} g, a 200 km asteroid, over the disk-hosting lifetime of a WD. However, dusty WDs show accretion rates of up to 10^{11} g s $^{-1}$ (Dufour et al. 2012). To explain the observed high accretion rates, Rafikov (2011b) and Metzger et al. (2012) propose a runaway accretion scenario, where rapid transport of metals from the disk results from interaction between spatially coexisting dust and gas disks. In this scenario, a WD accretes 10^{22} g of metals in 10^5 years. Hence, typical WDs may accrete up to 10^{24} g of metal over 10 Myr, the total time they host circumstellar disks. This is comparable to the mass of the dwarf planet Ceres and Pluto’s moon Charon. Of course, if the tidally disrupted object is icy, the total accreted mass may be significantly higher (although see Jura & Xu 2012). Therefore, the debris surrounding WDs is likely supplied through disruption of solar system asteroid analogs, moons, and dwarf planets.

5. CONCLUSIONS

We present near- and mid-infrared observations and a comprehensive study of the SEDs of a metallicity-unbiased sample of 117 DA WDs from the PG survey. Only five of our targets show excess radiation from debris disks, indicating a debris disk frequency of $4.3^{+2.7}_{-1.2}\%$ which fits in well with previous surveys of this kind. We interpret this frequency as a lower limit to the frequency of planets around the 1–7 M_{\odot} progenitor MS stars; an indirect result for the intermediate-mass regime in which conventional exoplanetary detection methods are insensitive. Alternatively, we interpret the observed frequency of disks as the fraction of time a WD accretes from its debris disks over the entire cooling age of the star. We estimate that typical WDs may accrete metals from several generations of disks for ~ 10 Myr, corresponding to accretion of metals up to 10^{24} g. This means

WDs are capable of accreting bodies as large as dwarf planets as well as solar system asteroid analogs.

This work is based, in part, on observations made with the *Spitzer Space Telescope*, which is operated by the Jet Propulsion Laboratory, California Institute of Technology under a contract with NASA. Support for this work was provided by NASA. The PAIRITEL is operated by the Smithsonian Astrophysical Observatory (SAO) and was made possible by a grant from the Harvard University Milton Fund, the camera loan from the University of Virginia, and the continued support of the SAO and UC Berkeley. The PAIRITEL project and J.S.B. are further supported by NASA/Swift Guest Investigator Grant No. NNG06GH50G. We thank M. Skrutskie for his continued support of the PAIRITEL project. The IRTF is operated by the University of Hawaii under Cooperative Agreement No. NNX-08AE38A with the National Aeronautics and Space Administration, Science Mission Directorate, and Planetary Astronomy Program. We thank A. Gianninas for his helpful comments, J. Farihi for useful discussions, and C. Blake, M. Skrutskie, and E. Falco for helping with the PAIRITEL observations. We also thank the referee, Marc Kuchner, for insightful suggestions.

REFERENCES

- Becklin, E. E., Farihi, J., Jura, M., et al. 2005, *ApJ*, **632**, L119
- Bergeron, P., Wesemael, F., Dufour, P., et al. 2011, *ApJ*, **737**, 28
- Bloom, J. S., Starr, D. L., Blake, C. H., Skrutskie, M. F., & Falco, E. E. 2006, in ASP Conf. Ser. 351, *Astronomical Data Analysis Software and Systems XV*, ed. C. Gabriel, C. Arviset, D. Ponz, & S. Enrique (San Francisco, CA: ASP), 751
- Bonsor, A., & Wyatt, M. C. 2012, *MNRAS*, **420**, 2990
- Bowler, B. P., Johnson, J. A., Marcy, G. W., et al. 2010, *ApJ*, **709**, 396
- Burgasser, A. J., Kirkpatrick, J. D., Reid, I. N., et al. 2003, *ApJ*, **586**, 512
- Burleigh, M. R., Clarke, F. J., & Hodgkin, S. T. 2002, *MNRAS*, **331**, L41
- Cushing, M. C., Vacca, W. D., & Rayner, J. T. 2004, *PASP*, **116**, 362
- Cutri, R. M., Skrutskie, M. F., van Dyk, S., et al. 2003, 2MASS All Sky Catalog of Point Sources (NASA/IPAC Infrared Science Archive)
- Debes, J. H., Hoard, D. W., Wachter, S., Leisawitz, D. T., & Cohen, M. 2011, *ApJS*, **197**, 38
- Debes, J. H., & Sigurdsson, S. 2002, *ApJ*, **572**, 556
- Debes, J. H., Walsh, K. J., & Stark, C. 2012, *ApJ*, **747**, 148
- Dufour, P., Kilic, M., Fontaine, G., et al. 2010, *ApJ*, **719**, 803
- Dufour, P., Kilic, M., Fontaine, G., et al. 2012, *ApJ*, **749**, 6
- Farihi, J., Becklin, E. E., & Zuckerman, B. 2005, *ApJS*, **161**, 394
- Farihi, J., Gänsicke, B. T., Steele, P. R., et al. 2012, *MNRAS*, **421**, 1635
- Farihi, J., Jura, M., & Zuckerman, B. 2009, *ApJ*, **694**, 805
- Farihi, J., Zuckerman, B., & Becklin, E. E. 2008, *ApJ*, **674**, 431
- Fazio, G. G., Hora, J. L., Allen, L. E., et al. 2004, *ApJS*, **154**, 10
- Girven, J., Gänsicke, B. T., Steeghs, D., & Koester, D. 2011, *MNRAS*, **417**, 1210
- Gould, A., & Kilic, M. 2008, *ApJ*, **673**, L75
- Graham, J. R., Matthews, K., Neugebauer, G., & Soifer, B. T. 1990, *ApJ*, **357**, 216
- Johnson, J. A., Aller, K. M., Howard, A. W., & Crepp, J. R. 2010, *PASP*, **122**, 905
- Jura, M. 2003, *ApJ*, **584**, L91
- Jura, M., Farihi, J., & Zuckerman, B. 2007, *ApJ*, **663**, 1285
- Jura, M., Farihi, J., & Zuckerman, B. 2008, *AJ*, **135**, 1785
- Jura, M., & Xu, S. 2012, *AJ*, **143**, 6
- Kalirai, J. S., Hansen, B. M. S., Kelson, D. D., et al. 2008, *ApJ*, **676**, 594
- Kennedy, G. M., & Kenyon, S. J. 2008, *ApJ*, **673**, 502
- Kilic, M., Brown, W. R., & McLeod, B. 2010, *ApJ*, **708**, 411
- Kilic, M., Farihi, J., Nitta, A., & Leggett, S. K. 2008, *AJ*, **136**, 111
- Kilic, M., Gould, A., & Koester, D. 2009a, *ApJ*, **705**, 1219
- Kilic, M., Kowalski, P. M., Reach, W. T., & von Hippel, T. 2009b, *ApJ*, **696**, 2094
- Kilic, M., Patterson, A. J., Barber, S., Leggett, S. K., & Dufour, P. 2012, *MNRAS*, **419**, L59
- Kilic, M., von Hippel, T., Leggett, S. K., & Winget, D. E. 2005, *ApJ*, **632**, L115
- Kilic, M., von Hippel, T., Leggett, S. K., & Winget, D. E. 2006, *ApJ*, **646**, 474
- Klein, B., Jura, M., Koester, D., & Zuckerman, B. 2011, *ApJ*, **741**, 64
- Klein, B., Jura, M., Koester, D., Zuckerman, B., & Melis, C. 2010, *ApJ*, **709**, 950
- Liebert, J., Bergeron, P., & Holberg, J. B. 2005, *ApJS*, **156**, 47
- Melis, C., Farihi, J., Dufour, P., et al. 2011, *ApJ*, **732**, 90
- Metzger, B. D., Rafikov, R. R., & Bochkarev, K. V. 2012, *MNRAS*, **423**, 505
- Mullally, F., Kilic, M., Reach, W. T., et al. 2007, *ApJS*, **171**, 206
- Rafikov, R. R. 2011a, *ApJ*, **732**, L3
- Rafikov, R. R. 2011b, *MNRAS*, **416**, L55
- Rayner, J. T., Toomey, D. W., Onaka, P. M., et al. 2003, *PASP*, **115**, 362
- Reach, W. T., Kuchner, M. J., von Hippel, T., et al. 2005, *ApJ*, **635**, L161
- Reach, W. T., Lisse, C., von Hippel, T., & Mullally, F. 2009, *ApJ*, **693**, 697
- Reach, W. T., Megeath, S. T., Cohen, M., et al. 2005, *PASP*, **117**, 978
- Schneider, J., Dedieu, C., Le Sidaner, P., Savalle, R., & Zolotukhin, I. 2011, *A&A*, **532**, A79
- Steele, P. R., Burleigh, M. R., Dobbie, P. D., et al. 2011, *MNRAS*, **416**, 2768
- Vennes, S., Kawka, A., & Németh, P. 2010, *MNRAS*, **404**, L40
- von Hippel, T., Kuchner, M. J., Kilic, M., Mullally, F., & Reach, W. T. 2007, *ApJ*, **662**, 544
- Williams, K. A., Bolte, M., & Koester, D. 2009, *ApJ*, **693**, 355
- Wright, E. L., Eisenhardt, P. R. M., Mainzer, A. K., et al. 2010, *AJ*, **140**, 1868
- Xu, S., & Jura, M. 2012, *ApJ*, **745**, 88
- Zuckerman, B., & Becklin, E. E. 1987, *Nature*, **330**, 138
- Zuckerman, B., & Becklin, E. E. 1992, *ApJ*, **386**, 260
- Zuckerman, B., Koester, D., Melis, C., Hansen, B. M., & Jura, M. 2007, *ApJ*, **671**, 872
- Zuckerman, B., Koester, D., Reid, I. N., & Hüensch, M. 2003, *ApJ*, **596**, 477
- Zuckerman, B., Melis, C., Klein, B., Koester, D., & Jura, M. 2010, *ApJ*, **722**, 725